Polarization wave at the onset of collective cell migration

Dietmar Oelz, Hamid Khataee, Andras Czirok, and Zoltan Neufeld

Phys. Rev. E **100**, 032403 — Published 5 September 2019

DOI: 10.1103/PhysRevE.100.032403

Polarization wave at the onset of collective cell migration

Dietmar Oelz[1], Hamid Khataee[1,*], Andras Czirok[2,3], and Zoltan Neufeld[1]

[1]School of Mathematics and Physics, The University of Queensland, St. Lucia, Brisbane, Queensland, Australia.
[2]Department of Biological Physics, Eotvos University, Budapest, Hungary
[3]Department of Anatomy and Cell Biology, University of Kansas Medical Center, Kansas City, Kansas, USA

August 23, 2019

Abstract

Collective cell migration underlies morphogenesis, tissue regeneration, and cancer progression. How the biomechanical coupling between epithelial cells triggers and coordinates the collective migration is an open question. Here we develop a one-dimensional model for an epithelial monolayer which predicts that after the onset of migration at an open boundary, cells in the bulk of the epithelium are gradually recruited into outward-directed motility, exhibiting travelling wave-like behaviour. We find an exact formula for the speed of this motility wave proportional to the square root of the cells' contractility, which accounts for cortex tension and adhesion between adjacent cells.

Introduction

Through collective cell motion, groups of cells move together, for example, during gastrulation, tissue vascularization, tumor invasion or wound healing [1–3]. Such multicellular motion can also be recapitulated in cell culture experiments. Studies investigating the motion of kidney epithelial [4, 5] or endothelial [6–8] cells, as well as immune cells in explanted lymph nodes [9] indicate an intriguing motion pattern, self-organized by the interplay of cell-cell interactions.

Studies on the directed expansion of an epithelial layer can investigate either a long-term expansion of a cell colony with free boundaries unfolding over several days or a shorter-term response initiated by removal of a barrier. While the long-term expansion is driven primarily by cell proliferation [10–12], the short-term response is dominated by directed migration of cells into the newly opened area [13, 14]. Cell displacements are guided by cell polarity, a complex of biochemical processes establishing a specific spatial pattern of intracellular signaling molecules [15], which is often explained by a positive feedback between actin polymerization and polarization signals that stabilize the leading edge of migrating cells [16–18].

Intercellular coordination of polarity is an intriguing, yet little understood process. The best understood biochemical signaling mechanism is the planar cell polarity pathway [19, 20] that couples spatially separated bistable intra-cellular states among adjacent cells [21, 22]. Endothelial cells were also reported to transmit cell polarity information utilizing membrane curvature [23]. Recent experiments further stresses the importance of mechanosensing (modulation of biochemical signalling processes by mechanical stresses) [24–27] in coordinating and especially in triggering cell motion.

Existing computational models have modelled the coordination between adjacent cells during the collectice migration [28–36]. However, how intra-cellular and inter-cellular mechanobiology regulates cell polarization and coordinated initiation of motion, and also influences the speed at which motility wave propagates through a monolayer of cells are not well understood. Here, we theoretically explore how a mechanism, which involves mechanical forces and biomechanical feedback in and in-between cells, is capable to propagate cell polarity during the expansion of an epithelial monolayer. We demonstrate that a minimal model of this process predicts a travelling wave that

transmits polarization information to the bulk of the monolayer. We derive closed-form equations for its shape and speed.

Results and Discussion

Particle model

We propose a one-dimensional model of interacting particles to study how cell motility is synchronised through an epithelial cell layer expanding into a "wound", an area devoid of cells. We start with a node-spring model of N cells (indices $i = 1, ..., N$) in which every cell is represented by its scalar position x_i and polarity a_i. Neighbouring cells are connected by elastic springs whose constant κ is a phenomenological parameter which we will call contractility. It accounts for both the stiffness of the cells mediated by their contractile cortex and the mechanical coupling between neighbouring cells mediated by adhesion proteins.
To represent the interplay between cell polarity, cell contractility, mechanical coupling, and actual cell motion, we model the cell velocities as the sum of the polarity-dependent motility $M(a_i)$ and the passive velocities due to elastic forces acting between adjacent cells [37, 38],

$$\frac{\mathrm{d}x_i}{\mathrm{d}t} = M(a_i) + \frac{1}{\eta}\left(F_{i,+} + F_{i,-}\right), \tag{1}$$

where the drag coefficient η accounts for cell-substrate adhesion, and can be interpreted as averaged effect of adhesion complexes undergoing permanent turnover [39]. $F_{i,+} = \kappa(x_{i+1} - x_i - l_0)$ is an assisting elastic force exerted by cell $i+1$ that pulls the cell i forward, while $F_{i,-} = -\kappa(x_i - x_{i-1} - l_0)$ is an elastic force exerted by cell $i-1$ that resists the migration of cell i (Fig. 1(a)). For the last and leading cells, we set $F_{1,-} = F_{N,+} = 0$. The constant l_0 is both, the initial and the equilibrium distance between adjacent cells; see Fig. 1(a). The motility function M is defined by a Hill function with half-saturation polarity $\alpha > 0$ ensuring a finite maximal cell speed $M_{\max}$, namely $M(a_i) = M_{\max} M_n(a_i)$ where $M_n(a_i) = a_i^n/(a_i^n + \alpha^n)$.
To describe self-sustained polarisation we adopt a previously proposed model [8] similar to the one recently employed in [14],

$$\frac{\mathrm{d}a_i}{\mathrm{d}t} = -\beta a_i + \gamma \frac{\mathrm{d}x_i}{\mathrm{d}t}\,, \tag{2}$$

where $1/\beta$ and γ represent the persistence time of polarisation and reinforcement of polarisation through actual motion [40], respectively. According to Equation (1) this latter effect includes up-regulation of polarity through mechanical stress [14, 27, 41]. It is qualitatively equivalent to earlier models in which cell polarity aligns with cell velocity due to the inherent asymmetry created in a moving cell [32, 42, 43]; review in [28].

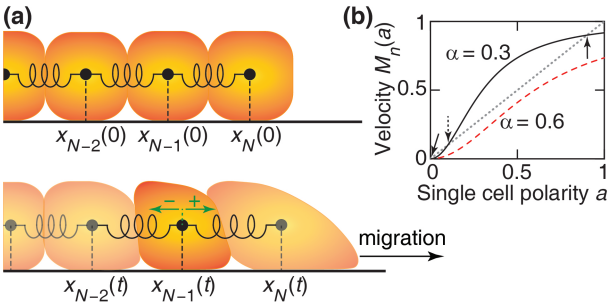

Figure 1: One-dimensional particle model. (a) Top: initially, cells are uniformly distributed and spaced at equilibrium distance at positions $x_i(0)$ and only the leading cell N is polarized. Bottom: elastic forces applied on a cell at time t. For example, cell $N-1$ feels force $F_{N-1,+}$ towards the cell-free surface (+, green arrow); and force $F_{N-1,-}$ in the backward (-, green arrow) direction. (b) Steady-state polarities of a single cell visualized as intersections of the active velocity $a^2/(a^2+\alpha^2)$(solid curves) and polarity a (gray dotted line). For half-saturation polarity $\alpha = 0.3$ (black) three steady-state polarities are: $a_1^* = 0$ (stable, solid arrow), $a_2^* = 0.1$ (unstable, dashed arrow), and $a_3^* = 0.9$ (stable, solid arrow). Thus, starting with an initial polarity greater than a_2^*, the cell will ultimately move with constant velocity and polarity. If α is too large, e.g. 0.6 (red dashed), there is no non-zero steady-state polarity.

We reduce the number of parameters in Equations (1) and (2) by defining the nondimensional variables $\widetilde{t} = \beta t$, $\widetilde{x}_i = (\beta/M_{\max})\, x_i$, $\widetilde{a}_i = (\beta/\gamma M_{\max})\, a_i$, and we introduce the two nondimensional parameters $\tilde{\alpha} = \alpha\beta/\gamma M_{\max}$ and $\tilde{\kappa} = \kappa/\beta\eta$. To keep the notation simple, we immediately remove the $\sim$ symbols. After non-dimensionalisation the model is given by

$$\begin{cases} \dfrac{\mathrm{d}x_i}{\mathrm{d}t} = \dfrac{a_i^n}{a_i^n + \alpha^n} + \kappa(x_{i+1} - 2x_i + x_{i-1}) \ , \\ \dfrac{\mathrm{d}a_i}{\mathrm{d}t} = -a_i + \dfrac{\mathrm{d}x_i}{\mathrm{d}t} \ . \end{cases} \tag{3}$$

Note that the motion of a single cell without adjacent cells is characterized by $\dot{x} = M(a)$ and $\dot{a} = -a + M(a)$. In this case, for a sufficiently low half-saturation polarity α, the single cell polarity has a bistable behavior: the stable rest state with zero polarity $a_1^* = 0$ coexists with a stable steady-state with constant non-zero polarity a_3^* (Fig. 1(b), solid arrows), and an unstable steady-state a_2^* (Fig. 1(b), dashed arrow), which separates the domains of attraction of the two stable states. Such bistable behavior has been experimentally observed in [17, 44]. We assume that the leading cell's polarity satisfies $a_N(t = 0) > a_2^*$, to mimic the migratory stimulus through the presence of a cell-free area to which the leading cell is exposed, while the trailing cells are initially unpolarised, $a_1(t = 0) = ... = a_{N-1}(t = 0) = 0$.
The numerical solution of Equations (3) shows that the polarization of the leading cell is propagated backward into the bulk of the epithelial layer; see Fig. 2(a,c), in agreement with recent experimental observations [13, 14, 34, 45, 46]. This is reminiscent of a travelling wave with a characteristic speed which we will call polarization wave speed.

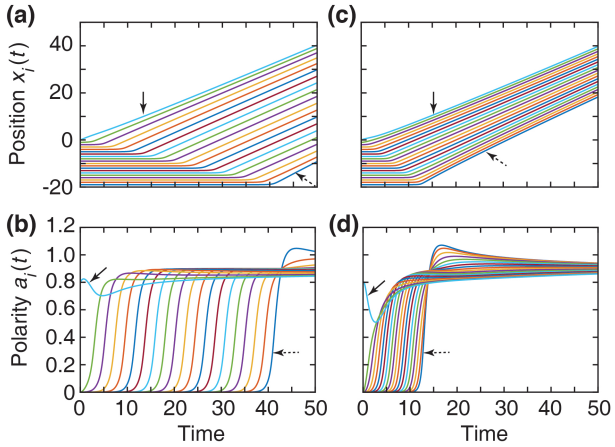

Figure 2: Migratory dynamics of a group of $N = 20$ cells obtained from the particle model with half-saturation polarity $\alpha = 0.3$ and Hill coefficient $n = 2$. The cells' displacement (top row) and polarity (bottom row) are shown versus time. Initially, only the leading cell (solid arrow, in contrast to dashed arrow showing last cell) is polarized, $a_{20}(0) = 0.8$, $a_1(0) = ... = a_{19}(0) = 0$. The cells' contractility is either weak (a, b: $\kappa = 0.1$) or strong (c, d: $\kappa = 1$) in which case polarization propagates significantly faster (compare a and c).

Simulations indicate that the polarization wave speed is faster if cells are more contractile (large κ); see Fig. 2(c,d). This agrees with the recent calculations by Bui et al. [36] that larger junctional force magnitudes are associated with faster collective cell migration. We also found that the polarization wave propagates faster for a lower half-saturation polarity value α. A lower α implies a lower polarization threshold a_2^* and therefore earlier switching from passive movement to active self-propelled motion.
To test the robustness of the results in Fig. 2, we extended the motility function $M(a)$ onto the negative domain as $M(-a) = -M(a)$ and included additive noise in Equation (2). This allows cells to polarize in either direction. The numerical results confirm that the overall behavior of the model remains the same, however the uni-directional migration is now superimposed onto a symmetric random movement; see Fig. 3.

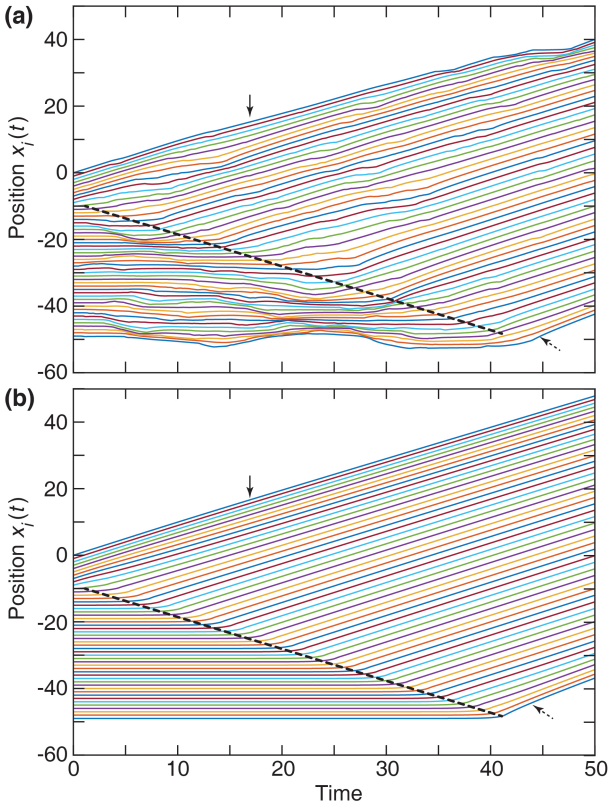

Figure 3: Position of $N = 50$ cells as a function of time derived from the particle model, when white noise ξ_i with magnitude ζ is added to Equation (2): $\mathrm{d}a_i/\mathrm{d}t = -\beta a_i + \gamma \mathrm{d}x_i/\mathrm{d}t + \zeta\,\xi_i$, for N cells with indices $i = 1, ..., N$. Simulation parameters are contractility $\kappa = 1$, half-saturation polarity $\alpha = 0.45$, Hill coefficient $n = 10$, and $\zeta = 0.45$ (a) and 0 (b), where the initial polarity of 10 cells close to the free edge are given by 0.8. The solid and dashed arrows point to the position of cells 50 (leading) and 1 (last). In the presence of random polarization direction, shown in (a), cells occasionally move backward. In both (a) and (b) the polarization wave propagates through the layer of cells with similar speed (dashed lines).

Continuum model

In order to use travelling wave analysis to compute the shape and speed of the polarization wave, we derive a continuum description of the particle model (3) whereby we model a population of cells with number density $\rho = \rho(x,t)$ moving along the x-axis according to the velocity field $v = v(x,t)$. The velocity changes the density through a continuity equation and the cell polarity $a(x,t)$ through transport,

$$\frac{\partial \rho}{\partial t} + \frac{\partial}{\partial x}(\rho v) = 0\,, \quad \frac{\partial a}{\partial t} + v\frac{\partial a}{\partial x} = -a + v\,. \tag{4}$$

To obtain the continuum description of the velocity field, we convert the distances between cell centers to density. Using $x_{i+1} - x_i = 1/\rho_{i+\frac{1}{2}}$, we re-write the expression for velocity in the system (3) as $\dot{x}_i = M_n(a_i) + \kappa(1/\rho_{i+\frac{1}{2}} - 1/\rho_{i-\frac{1}{2}})$. Multiplying and dividing the last bracket by $x_{i+1} - x_i = 1/\rho_{i+\frac{1}{2}}$, the continuum limit of velocity is

$$v = M_n(a) + \kappa\frac{1}{\rho}\frac{\partial}{\partial x}\left(\frac{1}{\rho}\right) = M_n(a) - \kappa\frac{1}{\rho^3}\frac{\partial \rho}{\partial x}\,. \tag{5}$$

Traveling wave analysis

To identify travelling polarity and density waves, we aim to solve the system (4) and (5) looking for solutions which can be written as fixed profiles with respect to a moving coordinate frame, $\rho(x,t) = R(z)$, $a(x,t) = A(z)$, where $z = x + ct$ parametrizes the wave profiles and $c > 0$ is the

wave speed. This way, $R = R(z)$ and $A = A(z)$ are the fixed profiles for density and polarity waves which propagate backwards into the monolayer of unpolarized cells at the constant speed c. They will be determined assuming that: (i) the polarity wave profile A connects the two stable steady-states $a_1^* = 0$ and a_3^*, which characterize the single-cell dynamics (Fig. 1(b)), and (ii) the density wave profile R connects the density of resting cells with $R_{-\infty} = \rho_0$ at $z \to -\infty$ to the density of moving cells with R_∞ at $z \to \infty$; see Fig. 4(a,b).
Substituting the traveling wave ansatz in the system (4) and (5) we obtain $cR' + (R\,M_n(A))' - \kappa\left(R'/R^2\right)' = 0$ and $cA' + \left(M_n(A) - (\kappa/R^3)\,R'\right)(A'-1) + A = 0$. By integrating the first equation and determining the integration constant at $z \to -\infty$ (where $R \to \rho_0$ and $A \to 0$; Fig. 4(a,b)), we obtain $-c\rho_0 + cR + R\,M_n(A) = (\kappa/R^2)\,R'$. Using this expression we eliminate R' in the second equation and obtain the following dynamical system for the travelling wave profiles,

$$\begin{cases} R' = \dfrac{R^2}{\kappa}\left[R\big(c + M_n(A)\big) - c\rho_0\right], \\ A' = 1 - R\dfrac{1}{\rho_0}\left(\dfrac{1}{c}A + 1\right). \end{cases} \tag{6}$$

The steady states of the system (6) satisfy $M_n(A) = A$ and $R = \rho_0\, c/(A+c)$. Hence its fixed points are $(R_{-\infty}, A_{-\infty}) = (\rho_0, 0)$, $(R_2, A_2) = (\rho_0\, c/(c+a_2^*), a_2^*)$, and $(R_\infty, A_\infty) = (\rho_0\, c/(c+a_3^*), a_3^*)$, where $R_\infty < R_2 < R_{-\infty} = \rho_0$ and $a_1^* = 0 < a_2^* < a_3^*$, as shown in the context of single cell motility in Fig. 1(b). The linear stability analysis reveals that the stable fixed points, $(\rho_0, a_1^* = 0)$ and (R_∞, a_3^*), are saddle points, whereas (R_2, a_2^*) is a focus; see Fig. 4(c). We analyze the asymptotics of the dynamics of travelling density and polarity waves in the system (6) by examining the stability of the three fixed points $(R_{-\infty}, A_{-\infty}) = (\rho_0, 0)$, $(R_2, A_2) = (\rho_0 c/(c+a_2^*), a_2^*)$ and $(R_\infty, A_\infty) = (\rho_0 c/(c+a_3^*), a_3^*)$. To this end we evaluate the Jacobian of the system at those steady-states. The Jacobian of Equations (6) is:

$$J = \begin{bmatrix} \frac{1}{\kappa}\left(3cR^2 + 3R^2 M_n(A) - 2c\rho_0 R\right) & \frac{1}{\kappa}R^3 M_n'(A) \\ -\frac{1}{\rho_0}(\frac{A}{c} + 1) & -\frac{R}{\rho_0 c} \end{bmatrix},$$

The evaluation of the Jacobian J at the first steady-state $(R_{-\infty}, A_{-\infty}) = (\rho_0, 0)$ is given by

$$J_1 = \begin{bmatrix} \frac{c\rho_0^2}{\kappa} & 0 \\ -\frac{1}{\rho_0} & -\frac{1}{c} \end{bmatrix}.$$

The determinant ζ_1, trace χ_1, and discriminant σ_1 of J_1 are:

$$\zeta_1 = -\frac{\rho_0^2}{\kappa}, \quad \chi_1 = \left(\frac{c\rho_0^2}{\kappa} - \frac{1}{c}\right), \quad \sigma_1 = \left(\frac{c\rho_0^2}{\kappa} - \frac{1}{c}\right)^2 + \frac{4\rho_0^2}{\kappa}.$$

This implies that the fixed point $(R_{-\infty}, A_{-\infty}) = (\rho_0, 0)$ is a saddle point. We then evaluate Jacobian J_m for $m = 2$ and 3 at the second and third steady-states $(R_2, A_2) = (\rho_0 c/(c+a_2^*), a_2^*)$ and $(R_\infty, A_\infty) = (\rho_0 c/(c+a_3^*), a_3^*)$ as:

$$J_m = \begin{bmatrix} \frac{c^2\rho_0^2}{\kappa(c+a_m^*)^2}\left(3c + 3a_m^* - 2(c+a_m^*)\right) & \frac{c^3\rho_0^3 M_n'(a_m^*)}{\kappa(c+a_m^*)^3} \\ -\frac{1}{c\rho_0}(c + a_m^*) & -\frac{1}{c+a_m^*} \end{bmatrix},$$

where we used $M_n(a_m^*) = a_m^*$. The determinant, trace, and discriminant of the J_m are:

$$\zeta_m = \frac{c^2\rho_0^2(M_n'(a_m^*) - 1)}{\kappa(c+a_m^*)^2}, \quad \chi_m = \frac{c^2\rho_0^2 - \kappa}{\kappa(c+a_m^*)}, \quad \sigma_m = \chi_m^2 - 4\zeta_m.$$

In the limit of large Hill coefficient n the Hill function $M_n(A)$ becomes a step function. In this regime the polarity at steady-state $a_2^* \to \alpha$ and $M_n'(a_2^*) \to \infty$. This implies that $\sigma_2 < 0$ and the

eigenvalues of J_2 are complex conjugate such that (R_2, A_2) is a focus. This focus point is unstable when $c\rho_0 > \sqrt{\kappa}$, where $\chi > 0$ and becomes stable for $c\rho_0 < \sqrt{\kappa}$. Likewise, in (R_∞, A_∞), the steady polarity increases $a_3^* \to 1$ as $n \to \infty$. In addition $M_n'(a_3^*) \to 0$. This results in $\sigma_3 > 0$, i.e. the eigenvalues are real and have different signs, since $\zeta_3 < 0$. Thus, (R_∞, A_∞) is a saddle point.

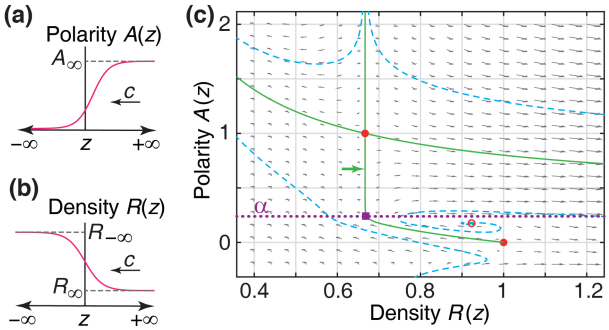

Figure 4: Travelling wave analysis. (a, b) Qualitative shapes of polarity A and density R wave profiles versus wave variable z. Rest state: $(R_{-\infty}, A_{-\infty})$; motile state: (R_∞, A_∞). Arrow shows the direction of the polarization wave speed c. (c) Phase diagram of the system (6) for a set of parameters ($\alpha = 0.2$, $n = 10$, $\kappa = 1$, $\rho_0 = 1$) and the approximately corresponding wave speed $c = 2$ obtained from Equation (9). The system exhibits a heteroclinic orbit (green solid curves) corresponding to the travelling wave profiles. Red closed circles: saddle points; red open circle: the focus; purple square: (R_∞, α). Additional trajectories (blue dashed) are depicted.

Our goal is to determine the polarization wave speed c such that the dynamical system (6) exhibits a heteroclinic orbit connecting the two saddle nodes, which corresponds to the continuous transition from the non-motile cell state to the motile state. We are not aware of explicit solutions of Equations (6) for a general Hill-function $M_n(A)$. In the limit $n \to \infty$, however, $M_n(A)$ becomes a step function and the phase space splits into two domains, where either $M_\infty = 0$ (for $A < \alpha$) or $M_\infty = 1$ (for $A > \alpha$). In both domains, the equations for the density and polarity profiles are decoupled and can be solved explicitly. On the domain $A > \alpha$, the stable manifold of the saddle point at (R_∞, A_∞) is a straight trajectory (Fig. 4(c), green arrow). Therefore, we know the coordinates of the point where the trajectory leaves the domain $A < \alpha$ (Fig. 4(c), purple square). We normalize the wave variable z such that the trajectory crosses the interface between the domains at $z = 0$, i.e. $R(z = 0) = R_\infty = \rho_0 c/(c + 1)$ and $A(z = 0) = \alpha$ (Fig. 4(c), purple square). We then introduce the rescaled density $P(z) = R(z)/\rho_0$ and re-write the system (6) on the domain $A < \alpha$ as,

$$P' = \frac{c\,P^2}{\chi}(P - 1)\,, \quad A' = 1 - P\left(\frac{1}{c}A + 1\right)\,, \tag{7}$$

where we temporarily use the short notation $\chi = \kappa/\rho_0^2$. The solution for the first equation in the system (7), with terminal condition $P(0) = c/(c + 1)$, is $P(z) = g^{-1}(cz/\chi + M)$, where $g(y) = 1/y + \log(1/y - 1)$ and $M = 1 + 1/c - \log(c)$ (see Fig. 5).

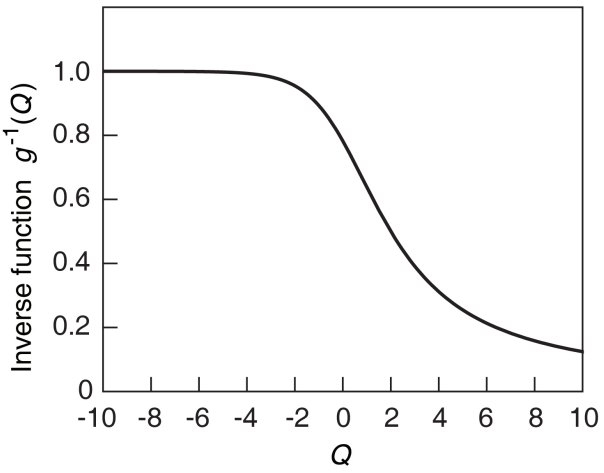

Figure 5: Inverse function $g^{-1}(Q)$ for $g(y) = 1/y + \log(1/y - 1)$.

Substituting this solution into the second equation in the system (7), coupled to the terminal condition $A(0) = \alpha$, yields

$$A(z) = \frac{c}{c^2/\chi + 1}\left(\frac{1}{g^{-1}\left(M + \frac{cz}{\chi}\right)} - 1\right) + \frac{\left(\alpha(c^2/\chi + 1) + c\right) g^{-1}(M) - c}{g^{-1}(M)(c^2/\chi + 1)}\left(\frac{\frac{1}{g^{-1}(M)} - 1}{\frac{1}{g^{-1}\left(M + \frac{cz}{\chi}\right)} - 1}\right)^{\frac{\chi}{c^2}}. \tag{8}$$

We recall our aim of constructing a heteroclinic orbit connecting the two saddle points; see Fig. 4(c). In the limit $z \to -\infty$, the density profile P tends to $P(-\infty) = 1$, but we also require that the polarity profile satisfies $A(-\infty) = 0$; see Fig. 5. The first term in (8) does satisfy this requirement. The second term, however, tends to $\pm\infty$, unless its leading factor vanishes. Therefore the requirement is $\left(\alpha(c^2/\chi + 1) + c\right) g^{-1}(M) - c = 0$. Using $g^{-1}(M) = c/(c+1)$ we conclude

$$c = \frac{1}{\rho_0}\sqrt{\kappa\left(\frac{1}{\alpha} - 1\right)}\,. \tag{9}$$

The formula (9) for the polarization wave speed agrees with numerical estimates based on the particle model, when varying either the contractility κ or the half-saturation polarity for $\alpha < 0.5$; see Fig. 6 and Fig. 7(a,b). Finally, reconstituting the physical dimensions of all quantities involved, the polarization wave speed reads

$$c = \frac{1}{\rho_0}\sqrt{\frac{\kappa\beta}{\eta}}\sqrt{\frac{\gamma M_{\max}}{\alpha\beta} - 1} \tag{10}$$

showing that the speed of retrograde movement of the boundary separating polarized and unpolarized cells is inversely proportional to the geometric mean of the characteristic mechanical response timescale (η/κ) and of the persistence time of the cell polarization $(1/\beta)$. Also, the asymptotic moving density written in physical dimensions is given by $\rho_\infty = \rho_0/(1 + M_{\max}/c)$, with c given by Equation (10). Having the wave speed c, the following explicit solutions for the polarity A and density R profiles define the shape of the polarization and density waves propagating with speed (9); see Fig. 7(c,d):

$$A(z) = \begin{cases} c\,\alpha\left(\frac{1}{g^{-1}\left(M + \rho_0^2\frac{cz}{\kappa}\right)} - 1\right) & z < 0 \\ 1 + (\alpha - 1)e^{-\frac{z}{1+c}} & z \geq 0 \end{cases} \tag{11}$$

and

$$R(z) = \begin{cases} \rho_0\, g^{-1}\left(\rho_0^2\frac{cz}{\kappa} + M\right) & z < 0 \\ \rho_\infty = \rho_0\frac{c}{c+1} & z \geq 0\,. \end{cases} \tag{12}$$

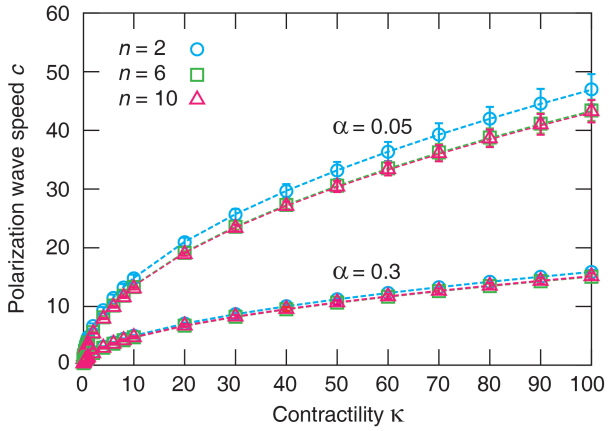

Figure 6: Polarization wave speed c versus cellular contractility κ. Speed c is derived from the particle model for $N = 2000$ cells in the contractility range $0.1 \leq \kappa \leq 100$ at two different values for half-saturation polarity $\alpha = 0.05$ and 0.3, each repeated for three different Hill coefficients $n = 2, 6$, and 10 (circle, square, and triangle symblos, respectively). Speed values correspond to mean $\pm$ SD. The dashed lines are the fits to the mean velocities. For $\alpha = 0.05$: $c = 4.71\sqrt{\kappa}$ (dashed blue), $c = 4.25\sqrt{\kappa}$ (dashed green), and $c = 4.23\sqrt{\kappa}$ (dashed magenta). For $\alpha = 0.3$: $c = 1.58\sqrt{\kappa}$ (dashed blue), $c = 1.48\sqrt{\kappa}$ (dashed green), and $c = 1.49\sqrt{\kappa}$ (dashed magenta).

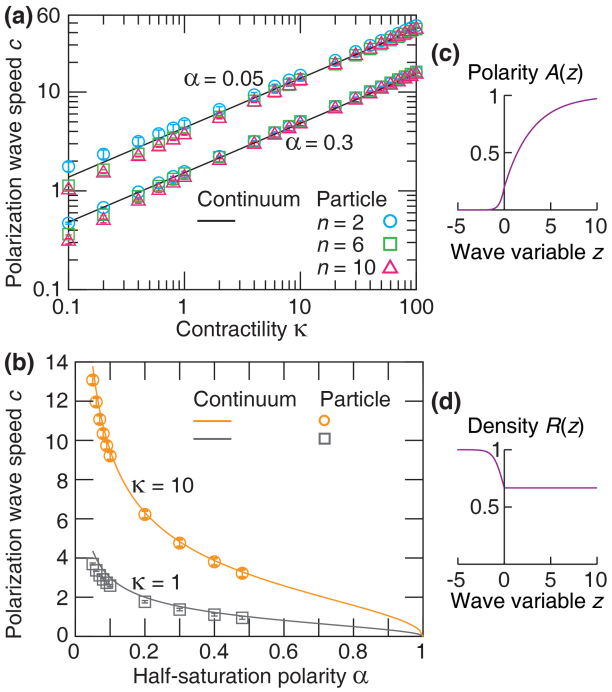

Figure 7: Comparison of the particle and continuum models. (a) Polarization wave speed c versus cells' contractility $0.1 \leq \kappa \leq 100$. Velocities (mean $\pm$ SD) are calculated by the particle model for $N = 2000$ cells at half-saturation polarities $\alpha = 0.05$ and 0.3, each repeated for Hill coefficients $n = 2, 6$, and 10 (circle, square, and triangle symbols, respectively). The output of the continuum model is derived from Equation (9) (black curves). Both models show that c is proportional to $\sqrt{\kappa}$, independently of n; as shown in Fig. 6. (b) Polarization wave speed c versus α. Particle and continuum models are run for two different κ, shown with symbols (mean $\pm$ SD) and solid curves, respectively. At $\alpha \geq 0.5$, the motility does not propagate into the interior of the cell layer in the particle model simulations; see Fig. 8. (c, d) Quantitative shapes of polarity and density wave profiles in the instantaneous polarization limit $n \to \infty$ (for formulas, see Equations (11, 12)).

Note, in the regime where the threshold for polarization is high, $\alpha > 0.5$, the polarization wave appears to be unstable and cannot be reproduced numerically. Instead a depolymerization wave

emerges; see Fig. 8.

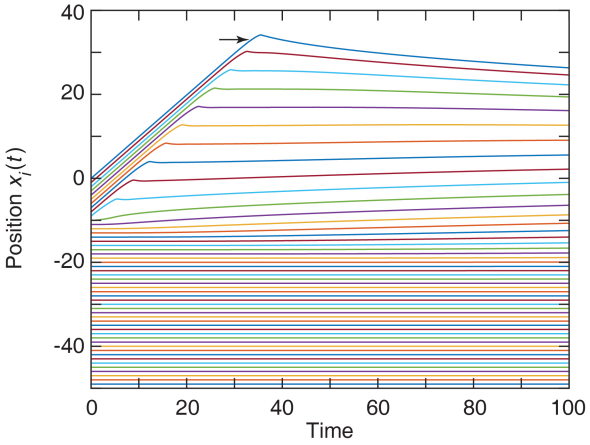

Figure 8: Position of cells versus time derived from the particle model for $N = 50$ cells with contractility $\kappa = 0.1$, half-saturation polarity $\alpha = 0.6$, and Hill coefficient $n = 10$, where the initial polarity of 10 cells from the leading edge were assigned as 0.8. The solid arrow points to the position of the leading cell 50. The motility wave does not propagate into the monolayer, as $\alpha > 0.5$. Instead, the trajectories exhibit a depolarization wave.

Equation (10) can be tested experimentally by perturbing epithelial cells in various ways. Perturbation of upstream regulators of the motor protein myosin-II could be used to test the dependence on contractility κ and/or on the efficiency of the motile machinery $M_{\max}$. One may also interfere with the coupling (adhesion and mechanosensitive feedback) between adjacent cells through genetic modification of the expression of e-cadherin, which – in the context of our 1D model – might affect both κ and the threshold for active motion α. Alternatively, one might focus on perturbing intracellular mechanisms driving and maintaining polarization which is reflected in the parameters β (persistence) and γ (polarization) instead.
Naturally, certain features of the expansion of the cell monolayer cannot be captured within the constraints of the one-dimensional model. For example, once the cell motility is activated the coherence of the collective migration is dependent on how well-ordered the alignment of the direction of cell polarization is maintained during migration. The alignment of the cell trajectories is likely to be sensitive to noise [47, 48] and to the mechanical coupling between cells. Among other things, it might affect how deep into the bulk of the cell sheet the polarization can reach. The edge of the cell sheet may also produce finger-like instabilities [49] which could also have an affect the wave of cell polarization. Those questions will have to be analyzed based on an extended two-dimensional model of epithelial collective migration.

Acknowledgments

DO was supported by ARC Discovery Project DP180102956. AC was supported by the NIH (GM102801) and the Hungarian National Research, Development and Innovation Office (ANN 118119). ZN was supported by ARC Discovery Project DP160104342.

References

[1]D. J. Montell, "Morphogenetic cell movements: diversity from modular mechanical properties", Science **322**, 1502–1505 (2008).

[2]P. Friedl and D. Gilmour, "Collective cell migration in morphogenesis, regeneration and cancer", Nat. Rev. Mol. Cell Biol. **10**, 445–457 (2009).

[3]E. Theveneau and R. Mayor., "Collective cell migration of epithelial and mesenchymal cells", Cell. Mol. Life Sci. **70**, 3481–3492 (2013).

[4]T. E. Angelini, E. Hannezo, X. Trepat, J. J. Fredberg, and D. A. Weitz, "Cell migration driven by cooperative substrate deformation patterns", Phys. Rev. Lett. **104**, 168104 (2010).

[5]S. Vedula, M. Leong, T. Lai, P. Hersen, A. Kabla, C. Lim, and B. Ladoux, "Emerging modes of collective cell migration induced by geometrical constraints", Proc. Natl. Acad. Sci. USA **109**, 12974–12979 (2012).

[6]J. H. Haga, "Molecular basis of the effects of shear stress on vascular endothelial cells", J. Biomech. **38**, 1949–1971 (2005).

[7]P. Vitorino and T. Meyer, "Modular control of endothelial sheet migration", Genes & development **22**, 3268–3281 (2008).

[8]A. Szabo, R. Unnep, E. Mehes, W. O. Twal, W. S. Argraves, Y. Cao, and A. Czirok, "Collective cell motion in endothelial monolayers", Phys. Biol. **7**, 046007 (2010).

[9]J. B. Beltman, A. F. Maree, J. N. Lynch, M. J. Miller, and R. J. de Boer, "Lymph node topology dictates T cell migration behavior", J. Exp. Med. **204**, 771–780 (2007).

[10]P. K. Maini, D. S. McElwain, and D. I. Leavesley, "Traveling wave model to interpret a wound-healing cell migration assay for human peritoneal mesothelial cells", J. Tissue Eng. **10**, 475–482 (2004).

[11]A. Puliafito, L. Hufnagel, P. Neveu, S. Streichan, A. Sigal, D. Fygenson, and B. Shraiman, "Collective and single cell behavior in epithelial contact inhibition", Proc. Natl. Acad. Sci. USA **109**, 739–744 (2012).

[12]M. J. Simpson, K. K. Treloar, B. J. Binder, P. Haridas, K. J. Manton, D. I. Leavesley, D. L. S. McElwain, and R. E. Baker, "Quantifying the roles of cell motility and cell proliferation in a circular barrier assay", J. Royal Soc. Interface **10**, 20130007 (2013).

[13]X. Serra-Picamal, V. Conte, R. Vincent, E. Anon, D. T. Tambe, E. Bazellieres, J. Butler, J. Fredberg, and X. Trepat, "Mechanical waves during tissue expansion", Nat. Phys. **8**, 628–634 (2012).

[14]S. Tlili, E. Gauquelin, B. Li, O. Cardoso, B. Ladoux, H. Delanoë-Ayari, and F. Graner, "Collective cell migration without proliferation: density determines cell velocity and wave velocity", Roy. Soc. Open Sci. **5**, 172421 (2018).

[15]Y. Mori, A. Jilkine, and L. Edelstein-Keshet, "Wave-pinning and cell polarity from a bistable reaction-diffusion system", Biophys. J. **94**, 3684–3697 (2008).

[16]A. Ridley, M. Schwartz, K. Burridge, R. Firtel, M. Ginsberg, G. Borisy, J. Parsons, and A. Horwitz, "Cell migration: integrating signals from front to back", Science **302**, 1704–1709 (2003).

[17]A. Lomakin, K. Lee, S. Han, D. Bui, M. Davidson, A. Mogilner, and G. Danuser, "Competition for actin between two distinct f-actin networks defines a bistable switch for cell polarization", Nat. Cell Biol. **17**, 1435–1445 (2015).

[18]R. Garner, E. Koslover, A. Spakowitz, and J. Theriot, "Stability on the edge: probing the biophysical mechanisms of polarity maintenance in motile cells", Biophys. J. **114**, 648a–649a (2018).

[19]R. S. Gray, I. Roszko, and L. Solnica-Krezel, "Planar cell polarity: coordinating morphogenetic cell behaviors with embryonic polarity", Dev. Cell **21**, 120–133 (2011).

[20]F. Bosveld, I. Bonnet, B. Guirao, S. Tlili, Z. Wang, A. Petitalot, R. Marchand, P. Bardet, P. Marcq, F. Graner, and Y. Bellaiche, "Mechanical control of morphogenesis by fat/dachsous/four-jointed planar cell polarity pathway", Science **336**, 724–727 (2012).

[21]Y. Burak and B. I. Shraiman, "Order and stochastic dynamics in drosophila planar cell polarity", PLOS Comput. Biol. **5**, 1–10 (2009).

[22]A. Asnacios and O. Hamant, "The mechanics behind cell polarity", Trends Cell Biol. **22**, 584–591 (2012).

[23]A. Hayer, L. Shao, M. Chung, L. Joubert, H. Yang, F. Tsai, A. Bisaria, E. Betzig, and T. Meyer, "Engulfed cadherin fingers are polarized junctional structures between collectively migrating endothelial cells", Nat. Cell Biol. **18**, 1311–1323 (2016).

[24]G. Charras and A. Yap, "Tensile forces and mechanotransduction at cell–cell junctions", Curr. Biol. **28**, R445–R457 (2018).

[25]B. Hoffman and A. Yap, "Towards a dynamic understanding of cadherin-based mechanobiology", Trends Cell Biol. **25**, 803–814 (2015).

[26]T. Lecuit and A. Yap, "E-cadherin junctions as active mechanical integrators in tissue dynamics", Nat. Cell Biol. **17**, 533–539 (2015).

[27]T. Das, K. Safferling, S. Rausch, N. Grabe, H. Boehm, and J. P. Spatz, "A molecular mechanotransduction pathway regulates collective migration of epithelial cells", Nat. Cell Biol. **17**, 276–287 (2015).

[28]B. A. Camley and W.-J. Rappel, "Physical models of collective cell motility: from cell to tissue", J. Phys. D: Appl. Phys. **50**, 113002 (2017).

[29]F. Graner and J. A. Glazier, "Simulation of biological cell sorting using a two-dimensional extended potts model", Phys. Rev. Lett. **69**, 2013–2016 (1992).

[30]A. G. Fletcher, J. M. Osborne, P. K. Maini, and D. J. Gavaghan, "Implementing vertex dynamics models of cell populations in biology within a consistent computational framework", Prog. Biophys. Mol. Biol. **113**, 299–326 (2013).

[31]A. G. Fletcher, M. Osterfield, R. E. Baker, and S. Y. Shvartsman, "Vertex models of epithelial morphogenesis", Biophys. J. **106**, 2291–2304 (2014).

[32]D. L. Barton, S. Henkes, C. J. Weijer, and R. Sknepnek, "Active vertex model for cell-resolution description of epithelial tissue mechanics", PLOS Comput. Biol. **13**, 1–34 (2017).

[33]N. Sepúlveda, L. Petitjean, O. Cochet, E. Grasland-Mongrain, P. Silberzan, and V. Hakim, "Collective cell motion in an epithelial sheet can be quantitatively described by a stochastic interacting particle model", PLOS Comput. Biol. **9**, 1–12 (2013).

[34]Y. Zhang, G. Xu, R. Lee, Z. Zhu, J. Wu, S. Liao, G. Zhang, Y. Sun, A. Mogilner, W. Losert, and T. Pan, "Collective cell migration has distinct directionality and speed dynamics", Cell. Mol. Life Sci. **74**, 3841–3850 (2017).

[35]C. Zmurchok, D. Bhaskar, and L. Edelstein-Keshet, "Coupling mechanical tension and GTPase signaling to generate cell and tissue dynamics", Phys. Biol. **15**, 046004 (2018).

[36]J. Bui, D. E. Conway, R. L. Heise, and S. H. Weinberg, "Mechanochemical coupling and junctional forces during collective cell migration", Biophys. J. **117**, 170–183 (2019).

[37]P. J. Murray, C. M. Edwards, M. J. Tindall, and P. K. Maini, "From a discrete to a continuum model of cell dynamics in one dimension", Phys. Rev. E **80** (2009).

[38]R. E. Baker, A. Parker, and M. J. Simpson, "A free boundary model of epithelial dynamics", J. Theor. Biol, 1–14 (2018).

[39]L. Preziosi and M. Scianna, "Mathematical models of the interaction of cells and cell aggregates with the extracellular matrix", in *Mathematical models and methods for living systems* (Springer, Italy, 2016) Chap. 3.

[40]P. Maiuri, J. Rupprecht, S. Wieser, V. Ruprecht, O. Bénichou, N. Carpi, M. Coppey, S. De Beco, N. Gov, C. Heisenberg, and C. Crespo, "Actin flows mediate a universal coupling between cell speed and cell persistence", Cell **161**, 374–386 (2015).

[41]A. Zaritsky, E. S. Welf, Y.-Y. Tseng, M. A. Rabadán, X. Serra-Picamal, X. Trepat, and G. Danuser, "Seeds of locally aligned motion and stress coordinate a collective cell migration", Biophys. J. **109**, 2492–2500 (2015).

[42]A. J. Kabla, "Collective cell migration: leadership, invasion and segregation", J. Royal Soc. Interface **9**, 3268–3278 (2012).

[43]B. Szabó, G. J. Szöllösi, B. Gönci, Z. Jurányi, D. Selmeczi, and T. Vicsek, "Phase transition in the collective migration of tissue cells: experiment and model", Phys. Rev. E **74**, 061908 (2006).

[44]A. B. Verkhovsky, T. M. Svitkina, and G. G. Borisy, "Self-polarization and directional motility of cytoplasm", Curr. Biol. **9**, 11–20 (1999).

[45]A. Zaritsky, D. Kaplan, I. Hecht, S. Natan, L. Wolf, N. Gov, E. Ben-Jacob, and I. Tsarfaty, "Propagating waves of directionality and coordination orchestrate collective cell migration", PLoS Comput. Biol. **10**, e1003747 (2014).

[46]K. Aoki, Y. Kondo, H. Naoki, T. Hiratsuka, R. E. Itoh, and M. Matsuda, "Propagating wave of erk activation orients collective cell migration", Dev. cell **43**, 305–317 (2017).

[47]R. Grima, "Multiscale modeling of biological pattern formation", Current topics in developmental biology **81**, 435–460 (2008).

[48] A. Middleton, C. Fleck, and R. Grima, "A continuum approximation to an off-lattice individual-cell based model of cell migration and adhesion", Journal of theoretical biology **359**, 220–232 (2014).

[49] V. Tarle, A. Ravasio, V. Hakim, and N. S. Gov, "Modeling the finger instability in an expanding cell monolayer", Integrative Biology **7**, 1218–1227 (2015).